



OPEN ACCESS

EDITED BY

Hao Shi,
Anhui University of Science and
Technology, China

REVIEWED BY

Chuanqing Fu,
Zhejiang University of Technology, China
Xiaoxiao Cao,
Kyushu University, Japan
Yiming Wang,
Suzhou University, China

*CORRESPONDENCE

Xianzhe Luo,
✉ 879056462@qq.com

RECEIVED 26 January 2025

ACCEPTED 03 March 2025

PUBLISHED 14 May 2025

CITATION

Li P, Luo X, Wang P, Wang K, Du Y and
Zhang Q (2025) Effect of CNT concentration
on mechanical properties and microstructure
evolution of grout.
Front. Mater. 12:1566974.
doi: 10.3389/fmats.2025.1566974

COPYRIGHT

© 2025 Li, Luo, Wang, Wang, Du and Zhang.
This is an open-access article distributed
under the terms of the [Creative Commons
Attribution License \(CC BY\)](https://creativecommons.org/licenses/by/4.0/). The use,
distribution or reproduction in other forums is
permitted, provided the original author(s) and
the copyright owner(s) are credited and that
the original publication in this journal is cited,
in accordance with accepted academic
practice. No use, distribution or reproduction
is permitted which does not comply with
these terms.

Effect of CNT concentration on mechanical properties and microstructure evolution of grout

Peng Li¹, Xianzhe Luo^{2*}, Pengyu Wang², Kai Wang², Yue Du²
and Qiang Zhang²

¹Shanxi Lu'an Mining (Group) Limited Liability Company Ancient City Coal Mine, Ltd., Changzhi, China,

²State Key Laboratory of Intelligent Construction and Healthy Operation and Maintenance of Deep Earth Engineering, China University of Mining and Technology, Xuzhou, Jiangsu, China

In order to elucidate the mechanism of carbon nanotubes (CNTs) in cementitious materials and their effects on microstructural and mechanical properties, this study combines in-house experiments with PFC^{2D} particle flow numerical simulations to systematically analyse the macromicro-mechanical behaviours of the grouted nodular bodies under different CNTs concentrations. Uniaxial compression tests were carried out on specimens constructed from crushed aggregate with a fractal dimension of 2.415, and the results showed that CNTs incorporation significantly enhanced the compressive strength and strain capacity of the nodules, with the optimal performance at a concentration of 0.05% CNTs, and the peak strength and peak strain were increased by 14.9% and 9.7% compared with those of the unincorporated specimens, respectively. Numerical simulation results showed that the maximum deviation of peak strength and strain between simulation and test was 2.01% and 2.96%, respectively, which verified the reliability of the model. Microanalysis showed that 0.05% CNTs optimised the crack extension path and force chain distribution by enhancing the bonding force at the cemented particle-aggregate interface, and inhibited the penetration of shear cracks, while too high a concentration (e.g., 0.15%) weakened the interface due to the agglomeration of CNTs, which exacerbated the force chain rupture and structural instability. This study reveals the regulation mechanism of CNTs concentration on the mechanical properties of the grouted rock body, which provides a theoretical basis for the efficient reinforcement of the crushed surrounding rock in engineering.

KEYWORDS

carbon nanotubes, cement-based materials, broken rock anchorage, particle flow model, mechanical property

1 Introduction

In deep underground engineering, the problem of the stability of the tunnel perimeter rock demands attention. The degree of broken perimeter rock with the deepening of the mining depth becomes more serious (Wu et al., 2025a), and the safety and stability of the perimeter rock has been challenged, presenting a more broken

state (Li et al., 2024; Wang et al., 2025) and seriously affecting the safety of lives and property (Wu et al., 2024). The structural characteristics of the fractured rock mass constitute the key factors governing the bearing capacity of the surrounding rock, and its structural characteristics have a central controlling effect on the deformation, damage, and destabilization mechanism of the surrounding rock (Han and Yang, 2009). Therefore, the study of methods to reinforce the broken rock to enhance the stability of the roadway-surrounding rock becomes the key to ensuring the safety of underground engineering.

Grouting material is widely used for the repair and strengthening of fractured surrounding rocks because of its high efficiency and economy. The performance of grouting materials is a key factor in determining the reinforcement effect (He and Lu, 2023). In selecting a grouting material, it is essential to consider factors such as the distribution of deformation damage to the roadway surrounding rock structure, the grouting process's capacity to enhance the deformation resistance of the consolidated body, and the cost-effectiveness of the process, particularly in terms of its adaptability to low-cost scenarios (Sun et al., 2022). The utilization of cementitious grouting materials in engineering practice is a prevalent solution for the repair of cracks, with the objective of enhancing the strength and stability of the rock body (Ren et al., 2022; Liu X. et al., 2024). These materials are characterized by their cost-effectiveness, ease of operation, and effectiveness. However, conventional cement-based grouting materials are not universally applicable due to their inherent limitations. The prevailing approach entails the incorporation of specific additives into cement-based grouting materials to address particular functional requirements, thereby enhancing their performance and compensating for their inherent limitations (He and Lu, 2024; Sha et al., 2024).

Carbon nanotubes (CNTs) are an innovative material in the nano field. Compared with graphene or silica nanoparticles, the high aspect ratio and bridging effect of CNTs can more effectively inhibit microcrack extension, making them a popular topic in many scientific research fields (Wu et al., 2025b). Research findings indicate that, within the domain of civil engineering, the synergistic composite of CNTs and cementitious materials has the potential to optimize the physical and mechanical properties of slurry materials to a significant degree (Wu et al., 2022). Moreover, the bridging function of CNTs (Nochaiya and Chaipanich, 2011; Wang et al., 2024) has been shown to enhance the interfacial transition region within the cement matrix, thereby significantly reducing the generation of microcracks and optimizing the overall performance of the material. Consequently, the internal structure of the grouting body is optimized (Parveen et al., 2013; Alafogianni et al., 2019), which enhances its application prospects in the field of crushed rock reinforcement (Shi et al., 2019). The incorporation of CNTs has been shown to enhance the mechanical properties of cementitious materials (Vafaeva and Zegait, 2024), and microscopic tests have revealed that the pore structure of cemented body specimens is improved by CNTs, making the structure more dense. The relationship between the incorporation of CNTs and the hydration product content of concrete was explored by thermogravimetric analysis. It was found that the incorporation of multiwalled CNTs led to a significant increase in the accumulation of calcium hydroxide in the concrete matrix (Carricho et al., 2018). This observation strongly corroborated the hypothesis that integrating multiwalled

CNTs could effectively accelerate the hydration process of cement and thereby promote the generation of hydration products.

Despite the considerable efforts of numerous scholars and experts in the field of grouting technology in fractured rocks, there are still many challenges to be addressed in this area. For instance, evaluating the grouting effect relies on extracting core samples to simulate the on-site reinforcement condition (Yao et al., 2024). However, it is difficult to accurately determine the exact proportion of each type of aggregate and its spatial distribution characteristics, which restricts the quantitative assessment of the effectiveness of the reinforcement and renders the results susceptible to uncertainty factors. Existing studies have mostly focused on the enhancement of macroscopic strength by CNTs, but their role in the micro-regulation of the chemical bonding mechanism and crack extension paths in the interfacial transition zone has not yet been clarified. Consequently, further in-depth studies are required to enhance comprehension and control of this process.

In this paper, starting from the laboratory experiment, the fractal dimension of an aggregate of different particle size ranges is described to quantify the fracture state of rock mass. The effects of changing CNT concentration on the mechanical properties of the consolidated body were determined. Then, using the method of numerical simulation, the discrete unit model of the consolidated body was constructed by using PFC2D software, and the aggregate particles with specific geometric characteristics were edited and imported into the model by using MATLAB programming skills. Finally, a highly simulated consolidated body model was obtained, and a mechanical test was carried out. Through this study, the influence of the change of CNT content on the grouting consolidated body at the microscopic level is systematically analyzed, which is helpful to deeply understand the interaction mechanism between CNTs and the grouting consolidated body, provide theoretical guidance for the design and preparation of building materials with better performance, and provide a reliable scientific basis for engineering practice.

2 Methods

2.1 Specimen preparation

In order to accurately assess the reinforcing efficiency of CNTs and promote their practical application in the field of damaged rock formation restoration engineering, it is necessary to select the ideal particle gradation that reflects the degree of damage to the crushed surrounding rock (Wu et al., 2020). In turn, the specific contribution of carbon nanotubes in enhancing rock stability is verified. The grading of fractured rock can be optimized using the relationship between ultrasonic pulse velocity and strength parameters (Wu et al., 2019), and the fractal dimension of the optimal aggregate size distribution fluctuates within the range of 2.4 and 2.6. Consequently, an aggregate with a fractal dimension of 2.415 was utilized in this test to characterize the current degree of crushing of the surrounding rock. The total mass of particles in the specimen was 300 g, the mold size was 50 mm (inner diameter) × 100 mm (height), and the specimen was maintained for 28 days. The specific aggregate particle size distribution and test program are shown in Tables 1, 2.

TABLE 1 Mass distribution of aggregate particles.

Fractal dimension	Aggregate particle mass in different size intervals (g)						
	0.25–1.0 mm	1.0–1.5 mm	1.5–2.5 mm	2.5–4.0 mm	4.0–6.0 mm	6.0–8.0 mm	8.0–10.0 mm
2.415	76.43	29.06	42.01	44.78	44.04	34.66	29.02

TABLE 2 Test plan.

Multiwalled CNT content (%)	Fractal dimension	Fly ash quality/cement quality	Slurry quality/aggregate quality	Water cement (cement and fly ash) ratio
0.00	2.415	0.25	0.53	0.75
0.05	2.415	0.25	0.53	0.75
0.10	2.415	0.25	0.53	0.75
0.15	2.415	0.25	0.53	0.75

Materials used in this test: cement is composite silicate cement (CPC 32.5); multiwalled CNT powder; fly ash density is 2.5 g/cm^3 ; aggregate gangue density is 2.72 g/cm^3 ; polycarboxylate-based water reducing agent model SHPC-101.

First, in this experiment, a multifunctional ultrasonic cell disruptor was used to disperse the carbon nanotubes, and a polycarboxylate-based water-reducing agent was added to assist the dispersion. The sonication time was 15 min. During ultrasonication, the beaker containing the dispersed solution was placed in ice water to eliminate the heat generated during the ultrasonication process, prevent it from affecting the carbon nanotube properties, and prepare uniformly distributed carbon nanotube solutions. Next, cement and fly ash were mixed thoroughly with a mixer, and then the prepared carbon nanotube aqueous dispersion was added while mixing for approximately 7 min. Finally, the prepared carbon nanotube cementitious grouting material was slowly poured into the mold containing the aggregate. After solidification, the molds were demolded and cured to obtain the consolidated body pattern.

2.2 Uniaxial compressive test

In order to accurately investigate the mechanical properties of the consolidated body specimens, the uniaxial compressive test was carried out using the MTS816 electro-hydraulic servo rock testing machine from China University of Mining and Technology (see Figure 1). During the test, the MTS816 electro-hydraulic servo rock testing machine adopts the displacement control mode. The loading is carried out at a stable loading rate of 0.1 mm/min , and the pre-contact pressure is set at 0.1 kN . This ensures strict control of the test conditions and high accuracy of the data acquisition. Key mechanical parameters such as axial stress, axial strain, and volumetric strain are automatically recorded in the MTS-816 system. Three specimens of each type were tested to determine the distribution of the test results.

2.3 Analysis of experimental results

Table 3 demonstrates the uniaxial compressive strength and peak strain of the consolidated body at different CNT concentrations. As is evident from the table, the compressive strength of the consolidated body specimens exhibited an increasing trend with an initial increase in CNT concentration, followed by a subsequent decrease, reaching its maximum at a CNT concentration of 0.05%, which is 14.9% higher than that of the undoped condition. The effects of varying CNT concentrations on the stress–strain of the consolidated body specimens are illustrated in Figure 2. The peak strains of the cemented body specimens without CNTs and with CNT concentrations of 0.05%, 0.10%, and 0.15%, respectively, were 0.0076, 0.00834, 0.00847, and 0.00847, which were enhanced by 9.7%, 11.4%, and 11.4%, respectively, compared with that of the unadded CNT consolidated body specimens. The findings demonstrate that incorporating CNTs enhances the peak stress of the consolidated body specimen, thereby enabling the specimen to withstand the applied load even in the presence of cracks and breakage, a phenomenon attributed to the bridging effect.

It is evident from these experiments that incorporating CNTs positively influences the strength and strain of the consolidated body, with optimal results observed at a CNT concentration of 0.05%. Subsequently, this paper will elaborate on the evolution of the microstructure of the consolidated body and establish a discrete element particle flow model to comprehensively elucidate the theoretical mechanism underlying this phenomenon.

2.4 Establishment of particle flow model of the CNT cement-based consolidated body

Particle Flow Code (PFC) is a simulation software based on the discrete element method (DEM) that allows

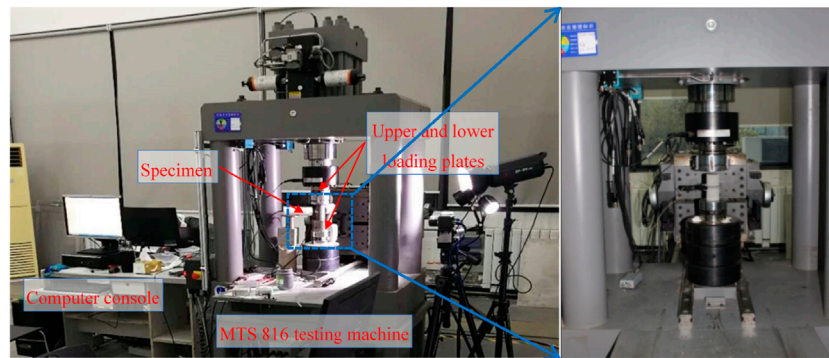


FIGURE 1 MTS-816 electro-hydraulic servo press.

TABLE 3 Uniaxial compressive test data table of different CNT concentrations.

Curing time	Multiwalled CNT content (%)	Peak stress/MPa	Peak strain
28	0.00	20.84	0.00760
	0.05	23.94	0.00834
	0.10	21.81	0.00847
	0.15	19.59	0.00847

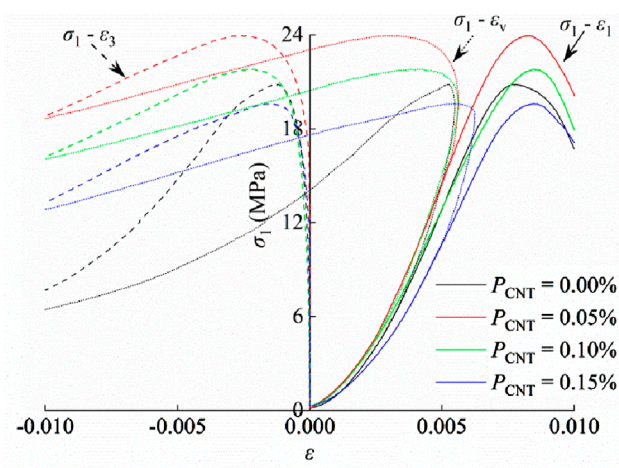
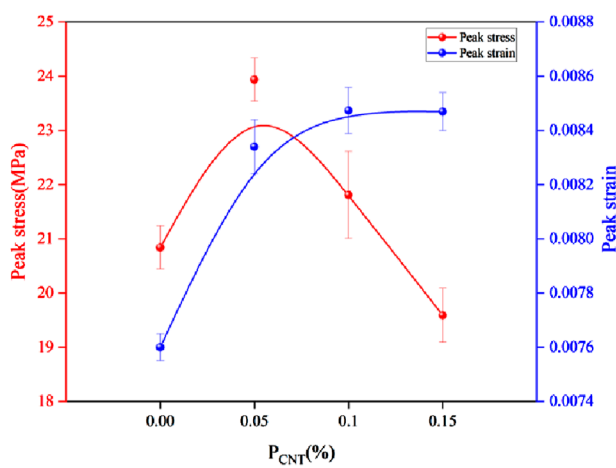


FIGURE 2 Effect of different CNT concentrations on the stress–strain curves of cemented specimens.

the iterative reproduction of the mechanical properties and damage mechanisms of materials under loads (Liu W. et al., 2024).

PFC avoids both the complexity of complex meshes in traditional methods and the complexity of setting intricate constitutive relationships for rock media. Its core lies in the accurate simulation of the contact between particles. By detecting the mechanical state of the contact surface, the process and internal

mechanism of particle damage and rupture can be determined. In this experiment, based on the above laboratory experiment data and by using PFC^{2D} particle flow numerical simulation software, a digital model of the consolidated body was constructed to simulate the dynamic evolution of particle failure, energy release history, force chain fracture phenomenon, and crack propagation characteristics. The law of changes of these key parameters with CNT concentration was systematically investigated.

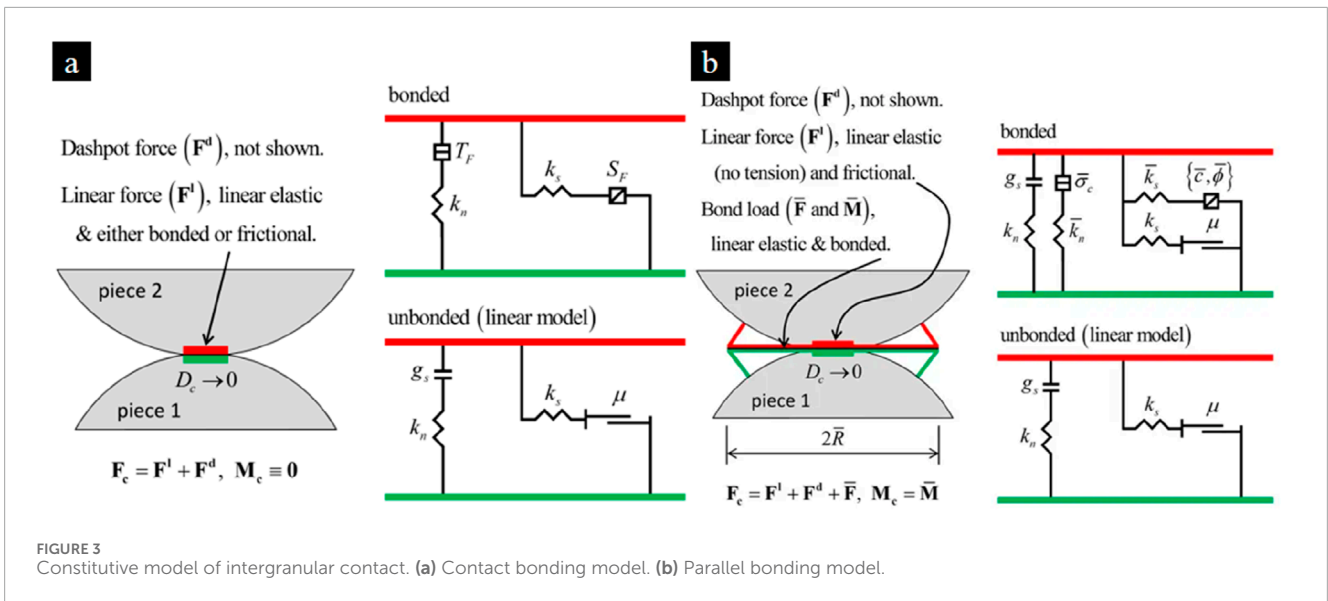


FIGURE 3 Constitutive model of intergranular contact. (a) Contact bonding model. (b) Parallel bonding model.

In the numerical simulation program PFC, the bond constitutive model is commonly used to simulate the bonding, fracture, and overall mechanical behavior of granular materials. The bond constitutive model is further subdivided into two distinct models: the contact bond model and the parallel bond model. These models are distinguished by their unique bond mechanisms and modes of action. The fundamental conceptual diagram of these two models is illustrated in Figure 3. In the field of rock mechanics, parallel bonding models are favored due to their ability to simulate bond strength and elasticity between particles, while also allowing slip and fracture of the bond interface under certain conditions. The parallel bond model describes the interaction between particles by defining the normal stiffness, shear stiffness, and bond strength of the contact surface. In this model, failure of the bond unit and destruction of the contact surface occurs when the force borne by the bond unit exceeds its maximum bond strength. This encompasses both the normal bond strength and the shear bond strength.

The model was used to analyze the effect of CNT concentration on the mechanical properties of consolidated body specimens. In the PFC^{2D} program, a sample with a height of 100 mm and a width of 50 mm was generated by the BALL command, and the numerical model comprised 21,341 particle units.

2.5 Analogy procedure

Following the consolidation of fractured rock, the resulting cemented specimen is typically a porous structure formed by the hydration products of the cementitious material, which encapsulate the aggregate. It is, therefore, imperative to distinguish between two media, cemented particles and aggregate particles, produced by cement hydration, and three contact surfaces: cemented particles, aggregate particles, and cemented-aggregate particles, when constructing particle flow models (Wu et al., 2021). The MATLAB programming language was utilized to generate aggregate particle models that were employed to regulate the mass and size distributions by implementing the particle

stacking stochastic reconstruction technique. The reconstruction method proposed in this study offers the distinct advantage of its enhanced resemblance to the reference model, thereby ensuring its applicability to any reconstruction of a granular structure. The main variables are the cumulative distribution function (cdf), aggregate volume fraction (volumFraction), storage particle size (particleSize), storage particle size random noise (noisy), store sample X-axis coordinate grid (sampleX), store sample Y-axis coordinate grid (sampleY), store sample polar angle grid (sampleTheta), and store sample rho grid (sampleRho). All arrays are single-precision, one-dimensional GPU arrays.

First, the coordinates of the center of the circle of particles were selected at the sample boundary to ensure a random distribution::

$$\begin{cases} X = \min(\text{sampleX}) + \text{randNum1} * [\max(\text{sampleX}) - \min(\text{sampleX})]. \\ Y = \min(\text{sampleY}) + \text{randNum2} * [\max(\text{sampleY}) - \min(\text{sampleY})] \end{cases} \quad (1)$$

The origin coordinate system was relocated to the center of the particle circle, after which it was transformed into a polar coordinate system:

$$[\text{sampleTheta}, \text{sampleRho}] = \text{cart2pol}(\text{sampleX} + X, \text{sampleY} + Y), \quad (2)$$

where cart2pol () is the built-in coordinate conversion function of MATLAB.

The average particle size \bar{X} is calculated using the particle size distribution function $\Psi(X)$ and the given random number $\xi \in [0, 1]$, sequence of particle sizes satisfying fractal features:

$$\bar{X}_\xi = \Psi^{-1}(\xi). \quad (3)$$

Random noise that varies with the polar angle is introduced to modulate the circular radius, thereby simulating the irregular shapes of aggregate particles as observed in reality and achieving an irregular particle radius distribution:

$$\text{noisy} = w \sum_{i=1}^n \frac{\text{randNum1}_i}{i} \sin(i * \text{sampleTheta} + 2\pi * \text{randNum2}_i), \quad (4)$$

where w is the coefficient that governs the magnitude of the radius noise, set to 0.1 in this study; n represents the number of noise terms, with a maximum value of n , and is set to 5 in this paper.

The final particle size X is

$$particleSize = \bar{X}_\xi \cdot (1 + noisy). \quad (5)$$

After determining the center coordinates and particle size using the aforementioned formula, the molecular density grid per unit volume of the particle compound is generated through conditional statements:

$$G = \{sampleRho \leq particleSize\}, \quad (6)$$

where G is the current particles of the aggregates grid.

The program progressively places particles within the sample space via an iterative process. In each cycle, a grid reflecting the current particle distribution is generated and superimposed on the grids from all preceding cycles:

$$G_N^{i+1} = G_N^i + \{sampleRho_i \leq particleSize_i\}. \quad (7)$$

During the iterative cycle, if a newly added aggregate particle overlaps with an existing particle area, the program will regenerate the particle placement until a non-overlapping location is identified. After each successful placement of an aggregate particle, the algorithm promptly updates the ratio of aggregate volume to sample volume and then dynamically adjusts its position until the volume fraction reaches the threshold value.

In consideration of the fundamental properties of the microstructure of the cemented filling medium, it was precisely imported into the particle flow model. From this model, a two-dimensional simulation model was constructed that exhibited a high degree of compatibility with the actual test and distinguished between two kinds of particles that had undergone reaction by cement hydration: cemented particles and aggregate particles. The model is shown in Figure 4. The cementitious medium is the product of cement hydration, which is assumed to be uniformly distributed cementitious particles. In contrast, the aggregate medium consists of aggregate particles aggregated to form clusters with geometrical characteristics. During the formation of cemented backfill, slurry and aggregate particles collaborate to form a porous structure. This structure is characterized by the complete encapsulation of aggregate particles by the cementing medium, which effectively mitigates friction and sliding between granular aggregates. The dense cementing matrix that envelops adjacent aggregates ensures each aggregate particle is thoroughly coated. Consequently, three types of interfacial contacts are established in the model: cemented particle-cemented particles, aggregate particle-aggregate particles, and cemented particle-aggregate particles. These interfaces are modeled using the parallel bonding approach, allowing them to resist friction even after bond failure. Given the varying mechanical properties of these different interfaces, distinct micromechanical parameters must be assigned to accurately describe the bonding and friction characteristics of each interface transition zone.

3 Analysis of numerical simulation results

3.1 Effect of CNT concentration on strength and strain of cement-based consolidated body

Figure 5 illustrates the experimental and simulated outcomes for varying concentrations of CNTs. A comparison between the experimental and simulated results reveals that the uniaxial compressive test results for different CNT concentrations closely align with the simulation data. Specifically, the maximum discrepancy in peak strength under uniaxial compression is only 0.4 MPa, representing a deviation of 2.01%. Similarly, the maximum difference in peak strain is 0.0024, corresponding to a deviation of 2.96%. This is a small deviation from the indoor uniaxial compression test results, indicating that the model accuracy meets the requirements. Detailed values from both the tests and simulations are presented in Table 4.

3.2 Effect of CNT concentration on the energy evolution of a cement-based consolidated body

For the roadway surrounding a rock system, the surrounding rock not only absorbs energy but also bears the critical responsibility of supporting the load from the overlying rock layers. Therefore, regulating the energy conversion mechanism between the cemented backfill and the overlying rock layer is essential for accurately controlling the deformation and displacement of the rock layers. Excluding dynamic effects, the total energy absorbed by the fractured rock reinforcement comprises the friction energy and the strain energy consumed by the structure in resisting deformation. This energy evolution law is also associated with damage evolution processes like crack development and force chain breakage.

Figure 6 illustrates the influence of CNT content on the strain energy characteristics of the consolidated body. As depicted in the figure, under conditions where structural stability is maintained, the peak strain energy exhibits a nonlinear trend characterized by an initial increase followed by a decrease at constant strain or stress levels. The inflection point occurs at a CNT content of 0.05%, where the strain energy reaches its maximum. This observation indicates that the addition of an optimal amount of CNTs significantly enhances the structural properties of the specimens due to the bridging effect of CNTs, which facilitates greater energy absorption. Subsequently, as the CNT concentration increases beyond this optimal point, the peak strain energy begins to decline. At a CNT concentration of 0.15%, the peak strain energy decreases markedly, only marginally exceeding that of specimens without CNTs. This suggests that excessive CNTs may adsorb water or compete with cement particles for reactive sites, leading to insufficient hydration product formation or incomplete microstructure, thereby adversely affecting the overall structural integrity (Alafogianni et al., 2019).

Figure 7 exhibits the effect of different CNT concentrations on the friction energy of the consolidated body specimen carrying the

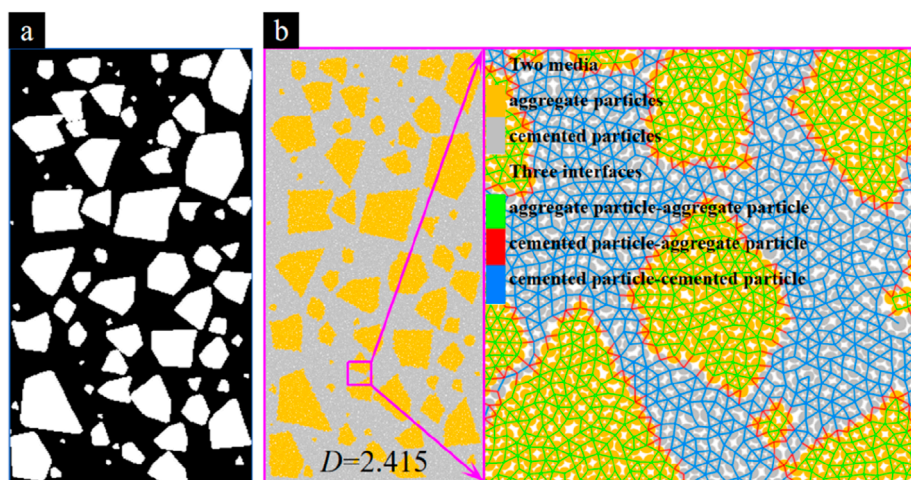


FIGURE 4 Consolidated body model. (a) Numerical model of the consolidated body. (b) Particle flow model for the consolidated body.

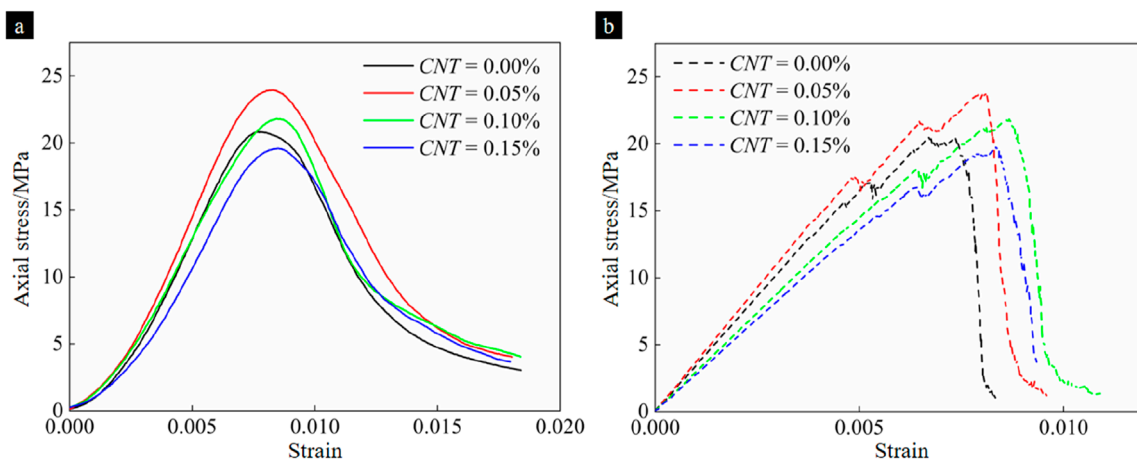


FIGURE 5 Comparative analysis of test and simulation results. (a) Uniaxial compressive test results of different CNT concentrations. (b) Uniaxial compressive simulation results of different CNT concentrations.

TABLE 4 Detailed values of experimental results and simulation outcomes.

Sample parameter	Peak stress test value (MPa)	Peak stress simulation value (MPa)	Percentage error	Peak strain test value	Peak strain simulation value	Percentage error
0.00%	20.84	20.43	2.01%	0.00760	0.00740	2.70%
0.05%	23.94	23.84	0.42%	0.00834	0.00810	2.96%
0.10%	21.81	21.84	0.14%	0.00847	0.00860	1.51%
0.1%	19.59	19.75	0.81%	0.00847	0.00840	0.83%

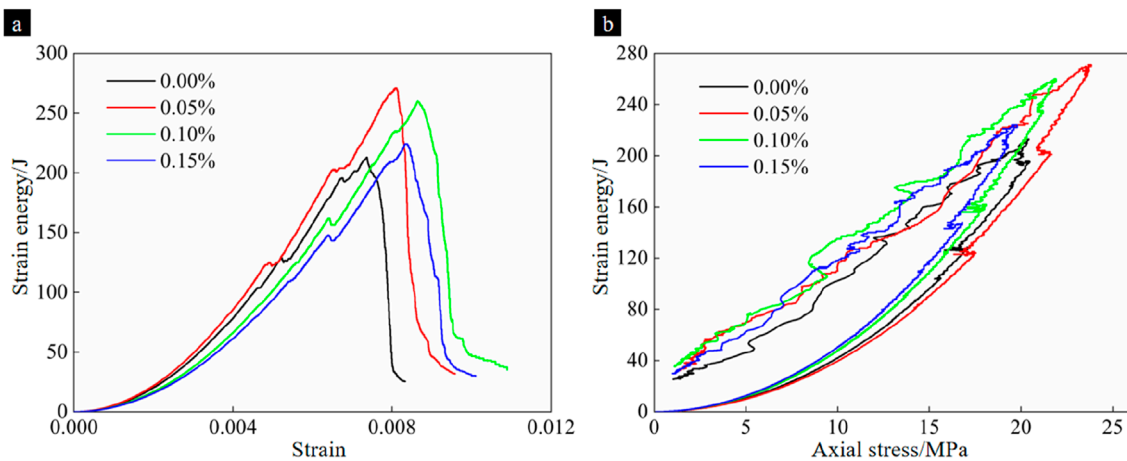


FIGURE 6 Influence of CNT concentration on the strain energy of the consolidated body. (a) Strain energy–strain of CNT concentration. (b) Strain energy–stress of CNT concentration.

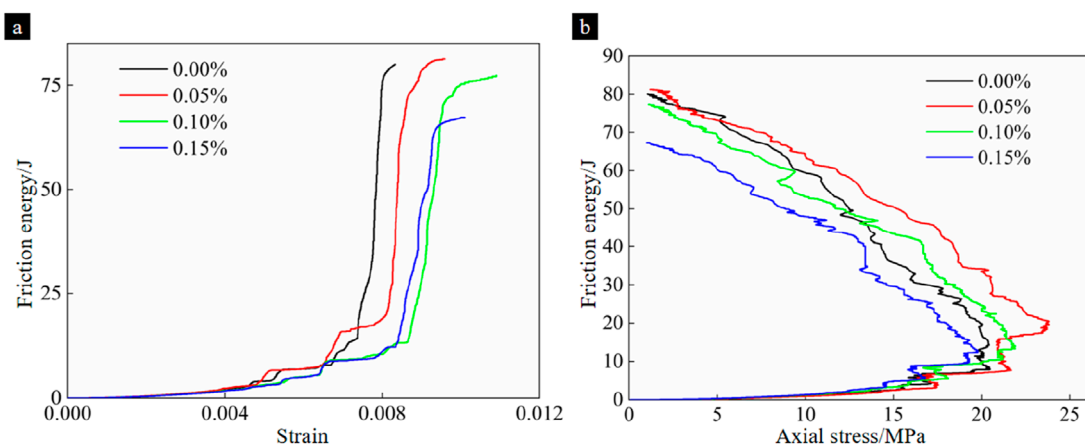


FIGURE 7 Influence of CNT concentration on the friction energy of the consolidated body. (a) Friction energy–strain of CNT concentration. (b) Friction energy–stress of CNT concentration.

whole load. It is important to note that while the friction energy of the consolidated body is not directly influenced by stress, it increases with increasing strain. The relationship curve between friction energy and CNT concentration, corresponding to peak strength and peak strain conditions, initially rises and then declines, reaching its maximum at a concentration of 0.05%. Samples with concentrations of 0.00% and 0.10%, respectively, exhibit lower friction energies. This indicates that an optimal concentration of CNTs can enhance the structural properties of the bulk sample. However, as the CNT concentrations increase beyond this point, the friction energy decreases, with the sample containing 0.15% CNTs showing the lowest value. This suggests that there is an optimum value for carbon nanotube concentration. Excessive CNT concentrations may have adverse effects on the structure of the consolidated body, potentially due to agglomeration.

3.3 Effect of CNT concentration on crack development of a cement-based consolidated body

The development of cracks in a consolidated body with varying CNT concentrations is illustrated in Figure 8. PFC particle flow model analysis shows that different concentrations of CNTs significantly influence the crack propagation modes in cemented samples. Under uniaxial compression, tensile cracks typically originate at the sharp corners of aggregates and, subsequently, propagate to other sharp corners or pre-existing cracks along the weakest regions at the interface between the aggregate and the cemented matrix. Simultaneously, shear cracks are mostly formed in the cemented matrix under greater shear force and develop along the path of higher shear stress. Figure 9 shows the relationship between

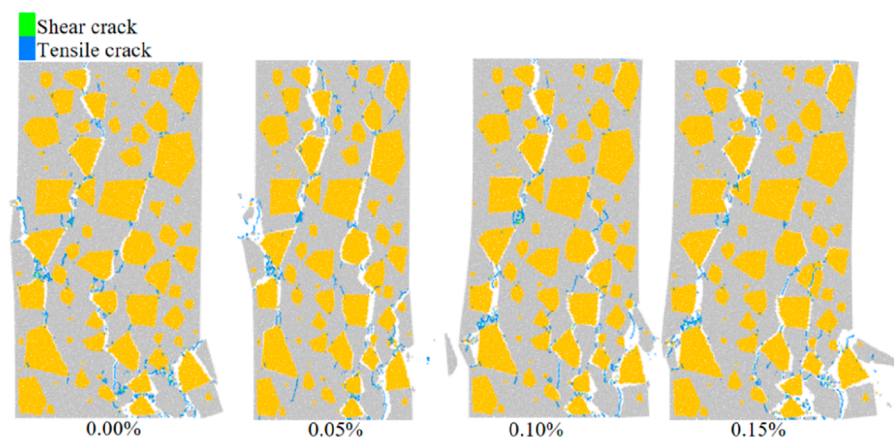


FIGURE 8
Effect of CNT concentration on crack distribution.

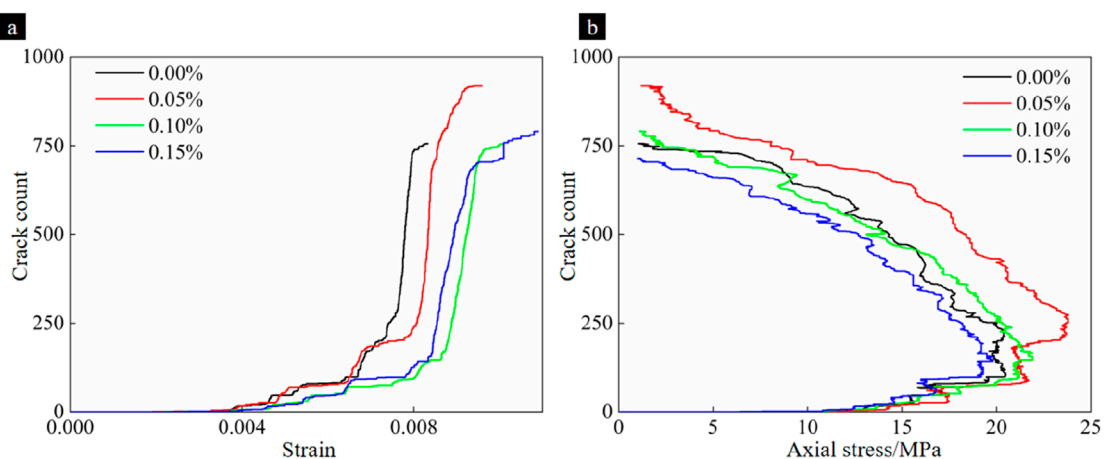


FIGURE 9
Influence of CNT concentration on crack development of the consolidated body. (a) Crack count–strain of CNT concentration. (b) Crack count–strain of CNT concentration.

the total number of cracks and the stress–strain at different CNT concentrations.

With the increase in CNT concentration, the development of cracks initially exhibited a trend of weakening before subsequently intensifying, predominantly at the sharp corners of the aggregate. This phenomenon suggests the existence of an optimal concentration of CNTs, with samples displaying minimal crack propagation at 0.05%. At this appropriate concentration, the strength of the binding matrix within the material is significantly enhanced, thereby strengthening the interface between cemented and aggregate particles. Consequently, even if initial cracks form at the aggregate's corners, they struggle to propagate further within the cementitious matrix. However, as the concentration of CNTs continues to rise, excessive amounts interfere with the hydration and hardening processes of the cement matrix, leading to an uneven internal structure. Agglomeration and inhomogeneous distribution cause uneven stress transfer within

the solidified body, leading to enhanced crack development in the specimen (Wu et al., 2022). This effect is particularly pronounced in samples with a CNT concentration of 0.15%. The crack development also echoes the energy evolution pattern above.

3.4 Effect of CNT concentration on force chain fracture of a cement-based consolidated body

Within the framework of Particle Flow Code, the force chain is regarded as an important index to characterize the interaction between particles. The dense layout of the force chain symbolizes the tightness and integrity of the structure and directly reflects the main bearing area of the structure. Through PFC^{2D} simulations and quantitative analyses (Figure 10), the regulatory mechanism of CNT

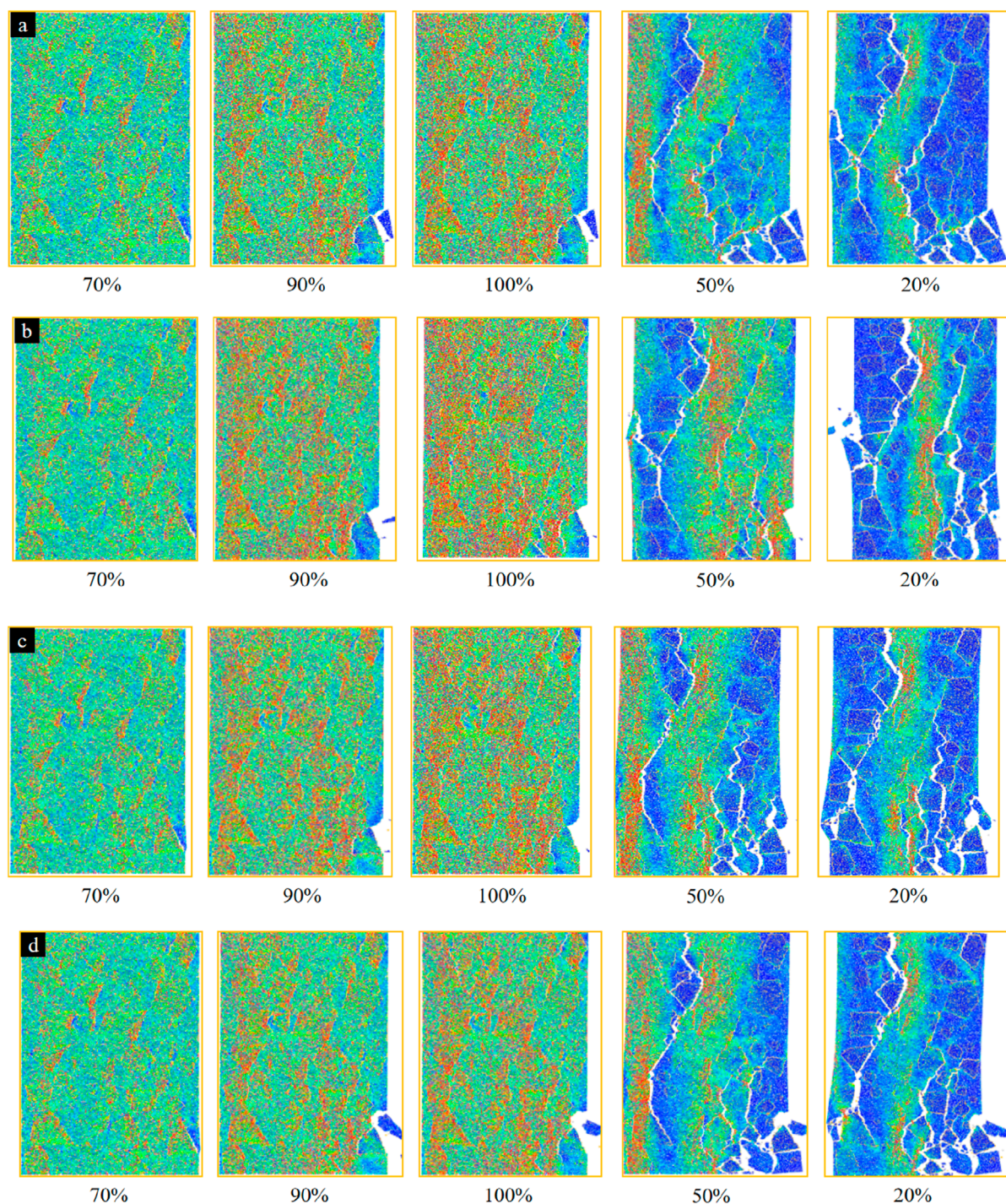
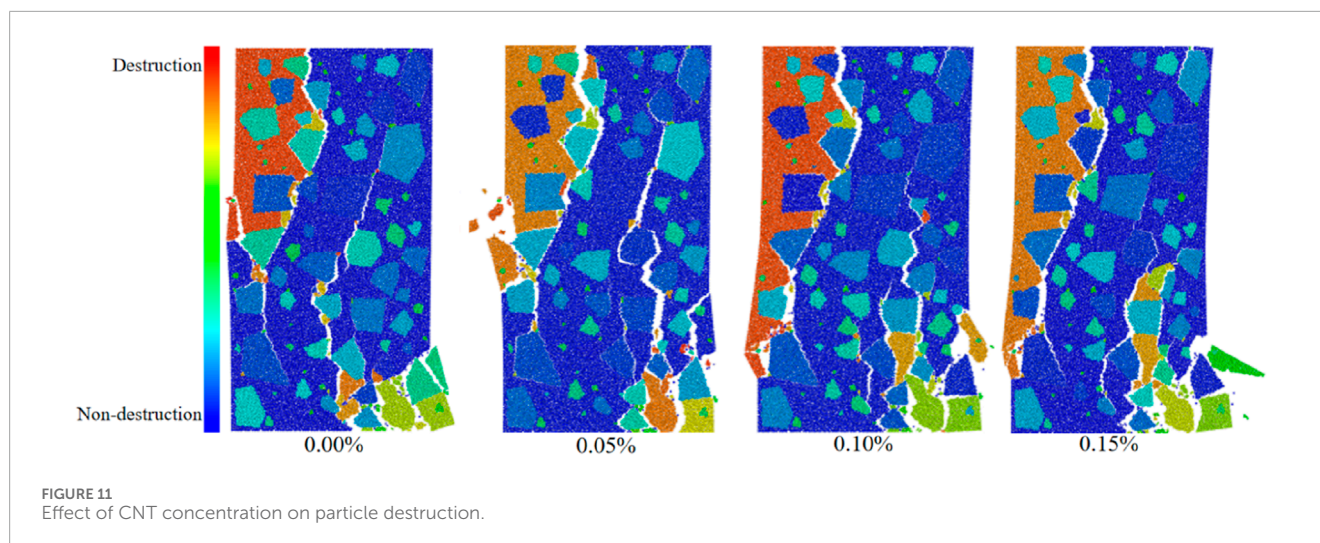


FIGURE 10
Effect of CNT concentration on force chain breakage. (a) CNT concentration 0.00%. (b) CNT concentration 0.05%. (c) CNT concentration 0.10%. (d) CNT concentration 0.15%.

concentration on the force chain rupture mode and structural load-bearing efficiency was revealed. To better illustrate the current load-carrying capacity of the specimen, the peak stress and its 90% and 70%, as well as 50% and 20% of the post-peak stress, were selected for analysis.

When the concentration of CNTs is 0.00%, the first signs of force chain rupture appear at the sharp right corner of the sample. With

the continuous accumulation of stress, the force chain fracture of the cementation–aggregate interface on this side is intensified, and the chain reaction of local failure leads to the deterioration of the bearing efficiency of the whole structure until it is fully permeated. After introducing an appropriate amount of CNTs (especially the 0.05% concentration), the bearing capacity of the sample is significantly improved, which not only enhances the contact surface between the



cemented particles and the aggregate particles but also optimizes the overall cementation characteristics of the grouting material. Under this ideal ratio, even under peak stress and post-peak half-load conditions, the samples did not show any force chain rupture originating from the sharp corner and associated damage to the cement-aggregate interface, which affected the structural load-bearing capacity of the structure. However, when the concentration of CNTs was increased to 0.15%, the force chain cracking at the sharp right corner increased steeply, and together with multiple force chain breaks within the cement, the overall degree of fracture was much higher than that in the case where no CNTs were added. It can be inferred that the force between the cement matrix and the particles is weakened when the concentration of CNTs is too high, which ultimately decreases the pressure-bearing capacity of the structure. This result most likely stems from the deterioration of the specimen due to the CNT agglomeration effect. The above phenomenon also echoes the law of energy evolution and crack development in consolidated bodies.

3.5 Effect of CNT concentration on particle destruction of a cement-based consolidated body

Figure 11 illustrates the influence of varying CNT concentrations on the damage patterns of consolidated body particles. As depicted in the figure, at a CNT concentration of 0.00%, the failure trajectory of the specimen originates from the aggregate's edge and subsequently propagates along the weakest cementation zones toward the sharp corners of the aggregate or near the fracture interface. Additionally, the swelling observed at the specimen's corners interconnects with the damage fractures, leading to a pervasive structural failure. However, as the concentration of CNTs gradually increased, the extent of damage to the specimen was markedly mitigated. At a concentration of 0.05% CNTs, while the failure path still adheres to the pattern from the most vulnerable cementitious region to the sharp angles or fracture boundaries of the aggregate, the magnitude of failure is substantially reduced compared to specimens without added CNTs. This

demonstrates that an appropriate concentration of CNTs can significantly enhance structural stability and strength. When the concentration of CNTs was increased to 0.15%, the extent of damage observed in the specimen exceeded that of specimens without CNTs. Continuous failure from the aggregate edge through the most vulnerable cementation layer to the aggregate tip or fracture surface became more pronounced, indicating that an excessively high concentration of CNTs adversely affects structural integrity. The high concentration of carbon nanotubes interferes with the hydration process of cement due to agglomeration and water-absorption effects, weakening the cementing matrix and the interface between the cemented particles and the aggregate particles and leading to a decrease in the structural load-bearing capacity. The above phenomena also correspond to the energy evolution mode, crack development, and force chain breakage in the cemented body.

4 Conclusion

In this study, aggregate particles with specified parameters were designed and generated through a combination of indoor experiments and numerical simulations utilizing MATLAB programming technology. A PFC^{2D} particle flow model was constructed to simulate the microstructural evolution of the consolidated body under loading conditions. The effects of CNT concentration on the mechanical properties and microstructural evolution of cement-based grouted consolidated bodies were systematically analyzed, revealing the mechanism of CNTs in the reinforcement of fractured surrounding rocks. The primary conclusions are:

- (1) The results demonstrate that incorporating an appropriate amount of CNTs substantially enhances the structural properties of the consolidated body. Notably, when the concentration of CNTs is 0.05%, both the uniaxial compressive strength and strain capacity achieve optimal values. The maximum deviation between the peak strength and experimental data is maintained within 2.01%, while the

maximum deviation between the peak strain and experimental data is kept within 2.96%. These findings validate the accuracy of the numerical simulation.

- (2) The specimens subjected to shear stress are more prone to developing shear cracks. An optimal concentration of CNTs (0.05%) can substantially enhance the strength of the bonding matrix within the material, thereby strengthening the interface between the cemented particles and the aggregate particles and inhibiting crack propagation. Conversely, an excessive concentration of CNTs may result in agglomeration, which can compromise the bonding strength between the cemented matrix and the aggregate particles and exacerbate crack development.
- (3) The influence of CNT concentration on the bearing performance of a consolidated body was investigated. The results indicate that an optimal concentration of CNTs (0.05%) significantly enhances the load-bearing capacity of the samples and optimizes the overall consolidation characteristics of the grouting material. Under conditions of peak stress and even at half-load post-peak, the degree of fracture in the force chains within the sample is minimal, thereby improving the structural load efficiency. Conversely, excessively high concentrations of CNTs can lead to force chain fractures at sharp corners or interfaces between aggregates that weaken the overall load-bearing capacity of the structure.

This study reveals the regulation mechanism of CNT concentration on the mechanical properties of grouted rock and provides a theoretical basis for the effective reinforcement of fractured surrounding rocks in engineering. With the increasing research on the properties and engineering applications of nanomaterials, CNTs are expected to drive innovative development in construction materials in a smarter, more sustainable, and efficient direction.

Data availability statement

The original contributions presented in the study are included in the article/supplementary material, further inquiries can be directed to the corresponding author.

References

- Alafogianni, P., Dassios, K., Tsakiroglou, C. D., Matikas, T. E., and Barkoula, N. M. (2019). Effect of CNT addition and dispersive agents on the transport properties and microstructure of cement mortars. *Constr. Build. Mater.* 197, 251–261. doi:10.1016/j.conbuildmat.2018.11.169
- Carriço, A., Bogas, J. A., Hawreen, A., and Guedes, M. (2018). Durability of multi-walled carbon nanotube reinforced concrete. *Constr. Build. Mater.* 164, 121–133. doi:10.1016/j.conbuildmat.2017.12.221
- Han, L., and Yang, M. (2009). Re-fracture process and mechanical characteristics of cracked rock samples. *Int. J. Rock Mech. Min. Sci.* 46, 738–747. doi:10.1016/j.ijrmms.2008.12.002
- He, R., and Lu, N. (2024). Air void system and freezing-thawing resistance of concrete composite with the incorporation of thermo-expansive polymeric microspheres. *Constr. Build. Mater.* 419, 135535. doi:10.1016/j.conbuildmat.2024.135535
- He, R., and Lu, N. L. (2023). Unveiling the dielectric property change of concrete during hardening process by ground penetrating radar with the antenna frequency of 1.6 GHz and 2.6 GHz. *Cem. Concr. Compos.* 144, 105279. doi:10.1016/j.cemconcomp.2023.105279
- Li, L., Jiang, Q., Huang, Q., Xiang, T., and Liu, J. (2024). Advances in stability analysis and optimization design of large underground caverns under high geostress condition. *Deep Resour. Eng.* 1, 100113. doi:10.1016/j.deepr.2024.100113
- Liu, W., Fan, H., and Huang, J. (2024a). Experimental and simulation study on failure mechanical characteristics of jointed underground roadway. *Comp. Part. Mech.* 11, 263–275. doi:10.1007/s40571-023-00621-x
- Liu, X., Wang, S., Liu, B., Liu, Q., Zhou, Y., Chen, J., et al. (2024b). Cement-based grouting material development and prediction of material properties using PSO-RBF machine learning. *Constr. Build. Mater.* 417, 135328. doi:10.1016/j.conbuildmat.2024.135328
- Nochaiya, T., and Chaipanich, A. (2011). Behavior of multi-walled carbon nanotubes on the porosity and microstructure of cement-based materials. *Appl. Surf. Sci.* 257, 1941–1945. doi:10.1016/j.apsusc.2010.09.030
- Parveen, S., Rana, S., and Fanguero, R. (2013). A review on nanomaterial dispersion, microstructure, and mechanical properties of carbon nanotube and nanofiber reinforced cementitious composites. *J. Nanomater.* 2013, 710175. doi:10.1155/2013/710175

Author contributions

PL: writing – original draft. XL: writing – review and editing. PW: writing – review and editing. KW: writing – review and editing. YD: conceptualization and writing – review and editing. QZ: writing – review and editing.

Funding

The author(s) declare that financial support was received for the research and/or publication of this article. This work was supported by the National Natural Science Foundation of China (No. 52074269). The authors gratefully appreciate this support.

Conflict of interest

Author PL was employed by Shanxi Lu'an Mining (Group) Limited Liability Company Ancient City Coal Mine, Ltd.

The remaining authors declare that the research was conducted in the absence of any commercial or financial relationships that could be construed as a potential conflict of interest.

Generative AI statement

The authors declare that no Generative AI was used in the creation of this manuscript.

Publisher's note

All claims expressed in this article are solely those of the authors and do not necessarily represent those of their affiliated organizations, or those of the publisher, the editors and the reviewers. Any product that may be evaluated in this article, or claim that may be made by its manufacturer, is not guaranteed or endorsed by the publisher.

- Ren, J., Zhao, H., Zhang, L., Zhao, Z., Xu, Y., Cheng, Y., et al. (2022). Design optimization of cement grouting material based on adaptive boosting algorithm and simplicial homology global optimization. *J. Build. Eng.* 49, 104049. doi:10.1016/j.jobbe.2022.104049
- Sha, F., Bu, M., Fan, R., Yang, N., and Zhang, L. (2024). Development and application of novel microfine cement-based grout. *Case Stud. Constr. Mater.* 20, e03167. doi:10.1016/j.cscm.2024.e03167
- Shi, T., Li, Z., Guo, J., Gong, H., and Gu, C. (2019). Research progress on CNTs/CNFs-modified cement-based composites – a review. *Constr. Build. Mater.* 202, 290–307. doi:10.1016/j.conbuildmat.2019.01.024
- Sun, Y., Zhang, P., Yan, W., Wu, J., and Yan, F. (2022). Grouting material development and dynamic grouting test of broken rock mass. *J. Mater. Civ. Eng.* 34, 04022072. doi:10.1061/(ASCE)MT.1943-5533.0004190
- Vafaeva, K. M., and Zegait, R. (2024). Carbon nanotubes: revolutionizing construction materials for a sustainable future: a review. *Res. Eng. Struct. Mater.* 10, 559–621. doi:10.17515/resm2023.42ma0818rv
- Wang, W., Ren, J., Ding, Z., and Liu, Q. (2025). Failure mechanisms and stability control principles of high geostressed deep mining structures: investigation by FDEM and field measurements. *Eng. Fail. Anal.* 169, 109233. doi:10.1016/j.engfailanal.2024.109233
- Wang, Y., Zhang, L., Han, B., Sun, S., Qin, Y., Han, X., et al. (2024). Advances in self-sensing cement-based composites containing nano materials for smart civil infrastructures. *Measurement* 230, 114514. doi:10.1016/j.measurement.2024.114514
- Wu, J., Feng, M., Ni, X., Mao, X., Chen, Z., and Han, G. (2019). Aggregate gradation effects on dilatancy behavior and acoustic characteristic of cemented rockfill. *Ultrasonics* 92, 79–92. doi:10.1016/j.ultras.2018.09.008
- Wu, J., Jing, H., Gao, Y., Meng, Q., Yin, Q., and Du, Y. (2022). Effects of carbon nanotube dosage and aggregate size distribution on mechanical property and microstructure of cemented rockfill. *Cem. Concr. Compos.* 127, 104408. doi:10.1016/j.cemconcomp.2022.104408
- Wu, J., Jing, H., Pu, H., Zhang, X., Meng, Q., and Yin, Q. (2021). Macroscopic and mesoscopic mechanical properties of cemented waste rock backfill using fractal gangue | Request PDF. *Chin. J. Rock Mech. Eng.* 40, 2083–2100. doi:10.13722/j.cnki.jrme.2021.0234
- Wu, J., Jing, H., Yin, Q., Yu, L., Meng, B., and Li, S. (2020). Strength prediction model considering material, ultrasonic and stress of cemented waste rock backfill for recycling gangue. *J. Clean. Prod.* 276, 123189. doi:10.1016/j.jclepro.2020.123189
- Wu, J., Wong, H. S., Zhang, H., Yin, Q., Jing, H., and Ma, D. (2024). Improvement of cemented rockfill by premixing low-alkalinity activator and fly ash for recycling gangue and partially replacing cement. *Cem. Concr. Compos.* 145, 105345. doi:10.1016/j.cemconcomp.2023.105345
- Wu, J., Yang, S., Williamson, M., Wong, H. S., Bhudia, T., Pu, H., et al. (2025a). Microscopic mechanism of cellulose nanofibers modified cemented gangue backfill materials. *Adv. Compos Hybrid. Mater* 8, 177. doi:10.1007/s42114-025-01270-9
- Wu, J., Yang, S., Wong, H. S., Yin, Q., Zhang, H., Chen, W., et al. (2025b). Reinforcement mechanisms of cellulose nanofibers on cemented rockfill: macroscopic, microscopic and molecular insights. *Constr. Build. Mater.* 466, 140192. doi:10.1016/j.conbuildmat.2025.140192
- Yao, Z., Li, M., Huang, S., Chang, M., and Yang, Z. (2024). Study on the impact of grouting reinforcement on the mechanical behavior of non-penetrating fracture sandstone. *Constr. Build. Mater.* 453, 139079. doi:10.1016/j.conbuildmat.2024.139079